A New Analysis of the IMO Video Meteor Database

Sirko Molau, Abenstalstr. 13, 84072 Seysdorf, sirko@molau.de

Motivation

Starting in 1999, a database of meteor records was created from automated single station video observations (Molau, 1991) of the IMO network. At the 2006 IMC, a first full analysis of the IMO Video Meteor Database based on roughly 190,000 meteors was presented. In the optical domain it was the first time, that a list of meteor showers was obtained automated, based on fully objective criteria only. For each shower, the activity interval, radiant position and drift, and an activity profile was obtained. A number of hitherto unknown showers were found as well. The corresponding analysis procedure was derived and explained in detail in Molau (2006). However, beside the successful application of the analysis procedure, also a number of weak points were detected.

As of 2008, the database had almost doubled, which made it worthwhile to repeat the analysis. However, these weak points were to be addressed first. This paper describes the problems in detail and presents solutions for them. In addition, a new meter shower list derived from the new full analysis of the IMO Video Meteor Database is given.

Weak points of the analysis procedure

The algorithm to automatically detect meteor showers from single station observations was described in detail in Molau (2006). Here, a short summary is given:

- Given that M is the set of meteors and R the set of radiants, at first the conditional probabilities P (M | R) is accumulated separately for each solar longitude interval in a three-dimensional coordinate system (right ascension, declination, velocity). This step is comparable to an automated run of the Radiant software (Arlt, 1992) for all possible solar longitudes and velocities.
- Now the local maxima in the probability distribution are determined in an iterative fashion. They represent possible meteor shower radiants.
- In the next steps, radiants with similar properties (position, velocity) in consecutive solar longitude intervals are connected to derive meteor showers.
- Finally, the detected meteor showers are identified based on IMO Working List of Meteor Showers and a list of known sporadic sources.

The following weak points were identified during the 2006 analysis:

- Comparability: As the effective observing time, field of view and limiting magnitude are unknown, the meteor shower activity is computed from the ratio of shower to sporadic meteors. That results in nice qualitative activity profile, but the activity of meteor showers cannot be compared quantitatively, because the observing geometry is not accounted for.
- Meteor counts: In the analysis, sliding solar longitude intervals are used, such that each meteor contributes twice to the analysis. As this effect was not accounted for, the number of meteors given for each shower was too high.
- Interference from nearby showers: In the iterative search procedure, first the strongest meteor shower is determined. Its meteors are removed from the data set, and then the second strongest shower is determined etc. When there are two showers of equal strength nearby (e.g. Taurids), the strongest shower “attracts” all meteors in-between the two radiants. This leads to interference in the activity graphs when both showers are equally strong.
- Meteor shower velocities: From single station observations, meteor shower velocities can only be derived indirectly with statistical procedures. In the 2006 analysis, the velocity of well-known fast meteor showers was systematically underestimated.
- Parameter estimation: For the accumulation of probabilities, a certain probability distribution function is applied. In the 2006 analysis, a Gaussian distribution with empirically estimated standard deviation was used. This time, the real distribution was to be derived from data.

Comparability

In order to scale meteor shower activity such that they can be compared with one another, it is important to care about the observing geometry. A factor that determins how many meteors become visible from a certain meteor shower, is the radiant altitude (or, strictly speaking, the sine of the radiant altitude). The higher the radiant is in the sky, the more meteors will we record.

To account for this effect, the concept of the observability function was introduced. By definition, the observability function is the average sine of the radiant altitude at night time (solar altitude <-9°). Beside the radiant position, it only depends from the solar longitude and the latitude of the observing site.

To explain the concept, let's have a look at the Quadrantids between solar longitude 282° and 284° at latitude 48° N (figure 1). The yellow graph shows the solar altitude at daytime, which reaches hardly 20° in early January. The night time at 48° N is shaded grey – is starts somewhat after sunset and lasts until short before sunrise. The sine of the altitude of the Quadrantid radiant is shown in red. It is well known, that the radiant is low in the horizon until about midnight, but raises rapidly towards morning. The average of the sine, i.e. the fraction of the red from the total grey area is 0.407. So, at 48° N the Quadrantids have an observation probability of roughly 40%. If they would show a constant zenithal rate and produce a hundred meteors in the course of the night, one would observe about 40 of them. In order to correct for that effect, each observed meteor is weighted with the inverse of the observability probability, i.e. each recorded Quadrantid meteor will get a weight 1/0.402≈2.5. Thus, 40 recorded Quadrantids will be counted as 100 in the analysis.
It should be noted at this point, that the weight is limited to a maximum of 100 to limit the impact of single meteors from hardly observable radiants.

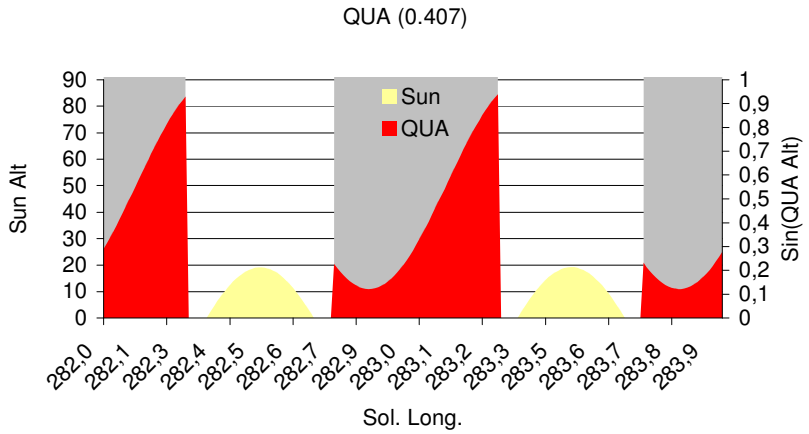

Figure 1: Observing geometry of the Quadrantids at solar longitude 282°-284° and latitude 48° N.

For comparison, figure 2 shows the observing geometry for selected well-known showers at the time of their maxima at latitude 48° N, sorted by the observation probability. The eta-Aquariids are hardly visible at 48° N (probability 0.032), whereas the Geminid radiant is well above the horizon all night long (probability 0.688).

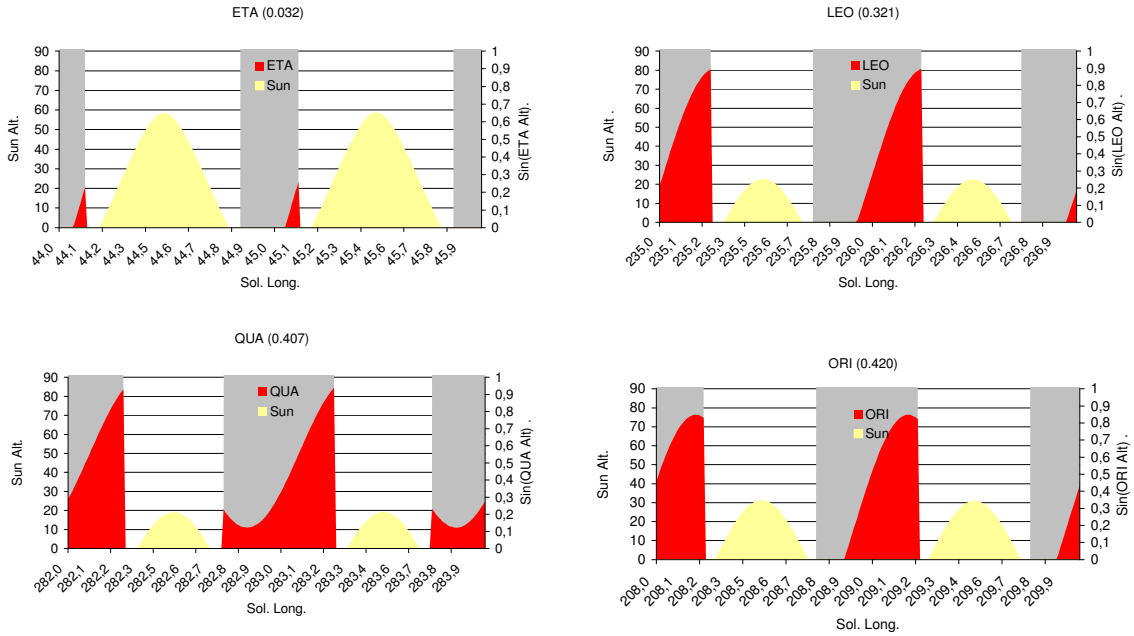

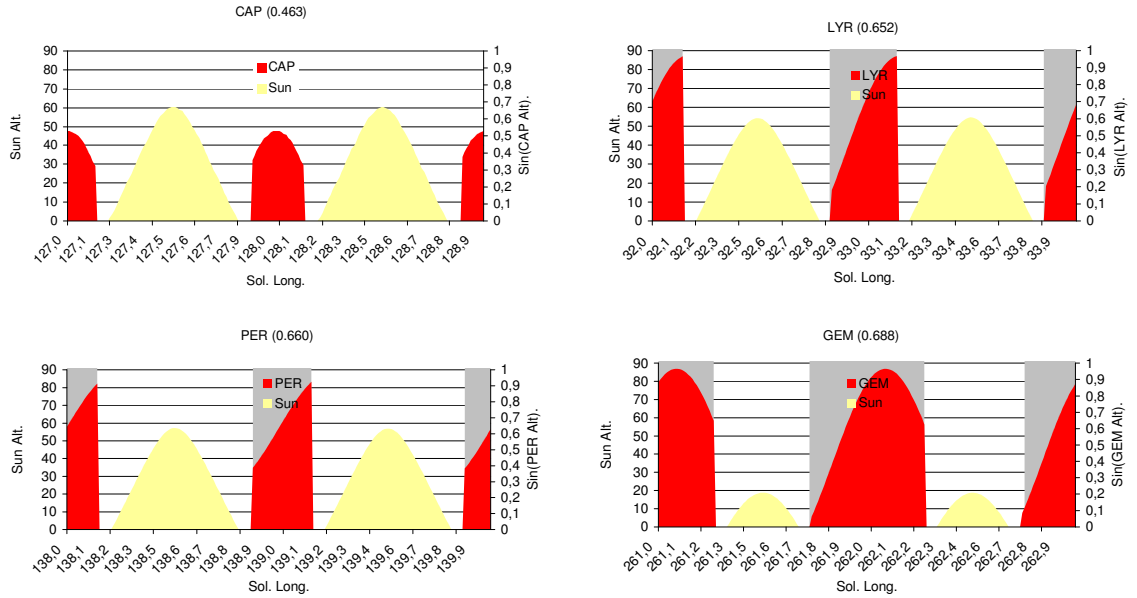

Figure 2: Observing geometry of selected well-known showers computed for the solar longitude of their maximum times and latitude 48° N

Beside the radiant position and the solar longitude, the observability function only depends on the latitude of the observing site, which makes the computation very efficient. Figure 3 gives the value of the observability function for the same showers as a function of the latitude. Note, that observing sites at mid-northern latitudes (48° N is marked with a vertical line) are well placed, because most showers have a large observability probability there. The sudden discontinuities in the graph result from the fact, that at a certain latitude the the Sun does not sink below –9° altitude anymore. The Capricornids are a fine example: The farther north the observing site, the shorter becomes the night time window and the smaller the grey area. Still, the observability function is not approaching zero, because within the smaller getting night time window the Capricornids still have a significant radiant altitude.

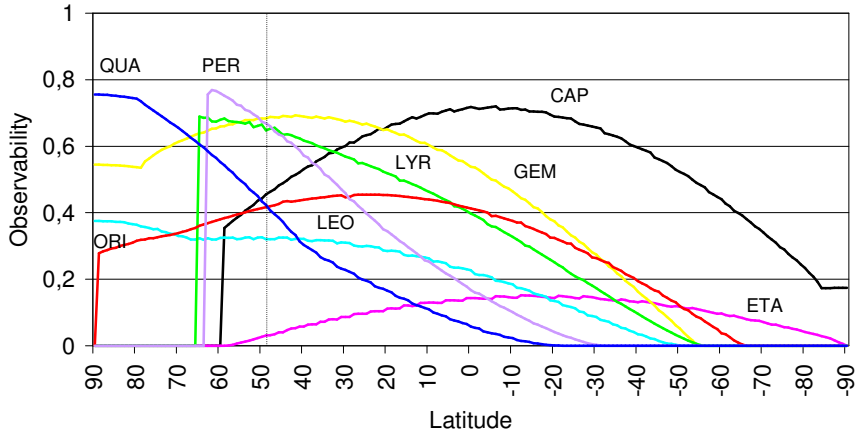

Figure 3: Observability function of selected showers at the time of their maximum as a function of the latitude.

There is one more effect to be considered: After application of the observability function, the meteor shower activity is obtained by dividing the number of shower and sporadic meteors. If data is collected over a long period, this will account quite well for variable observing conditions (limiting magnitude and field of view of the cameras, effective observing time). However, it does not account for annual variation of the sporadic activity. In northern hemisphere fall with strong sporadic activity, the meteor shower counts will be scaled down stronger than in sping time with low sporadic activity.

To account for this effect, the average hourly sporadic count was computed from the monthly statistics of the IMO network (figure 4). It turns out, that the activity A can be approximated by a sine function with a constant offset and a maximum at solar longitude S=170°:

$$A = 3.2 + \sin (S - 80°) \qquad [1]$$

This activity function is valid for the northern hemisphere only, but applied to all data, because only a small fraction of <10% from all data of the IMO Video Meteor Network are recorded at the southern hemisphere.

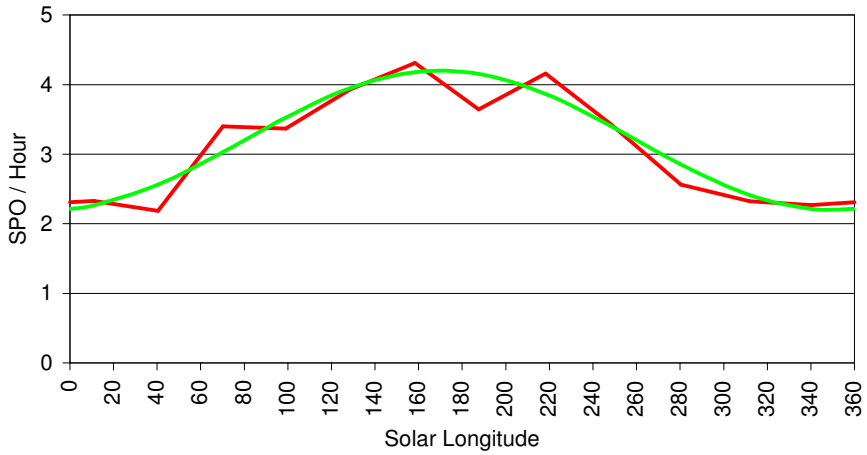

Figure 4: Average annular sporadic activity (red) computed from monthly statistics of the IMO network, and a sine function fitted to the data (green).

Applying the correction for annual sporadic activity variations will ensure that the meteor shower activity can now be compared for different showers. Still, the calculated activity has some arbitrary scaling. In order to get values that are similar to the visual ZHR, the sporadic counts were weighted, too. A fixed observability probability of 1/15 was choosen such that the eta-Aquariids activity reaches about 50 at the maximum.

Meteor Counts

Let's consider the situation for a shower that has been detected between solar longitude 43° and 47° (figure 5, left). The interval Sol43 contains all meteors from solar longitude 42° to 44°, the interval Sol44 all meteors from solar longitude 43° to 45°, and so on. Hence, all meteors between solar longitude 43° and 47° will be counted twice, but the meteor from solar longitude 42° to 43° and 47° to 48° not.
If the total number of meteors belonging to this shower is calculated, it is not sufficient to sum up the meteor counts of all intervals Sol43 to Sol47 and divide them by two, because errors will be introduced in the first and last interval. A simple solution is to store the number of meteors in the first and second half of each solar longitude interval independently (e.g. for Sol43 the number of meteors from 42°-43° and from 43°-44°). When the number of shower meteors is determined, all meteor counts but the first half of the first interval (Sol43) and the second half of the last interval (Sol47) will be divided by two.

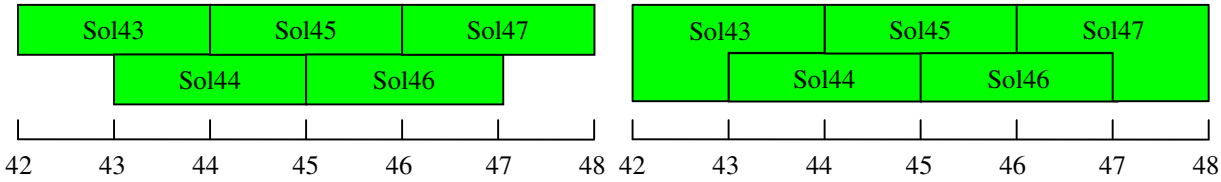

Figure 4: If sliding intervals are used, meteors in the first half of the fist interval, and the second half of the last interval will still contribute only once to the analysis of a meteor shower.

For one reason, the total number of meteors per shower is still slightly ambiguous: The radiant position in each solar longitude interval is slightly different. So there are cases where the same meteor is count as shower member in one interval, but not anymore in the following. However, that is just a marginal effect which can be neglected.

Interference from nearby showers

The interference in the activity graph of nearby meteor shower results from the iterative radiant search: When the strongest shower is determined, all meteors belonging to this shower are withdrawn and taken from the data set. It could be, that there is a weaker shower nearby, to which some meteors fit better, but that cannot be accounted for, as only the strongest shower is known at that time. In result, the strongest shower will "attract" all meteors nearby. When two nearby showers have about the same strength, at some time one or the other of these will be stronger, which will result in erratic jumps of the calculated activity (see Taurids in Molau, 2006).

The solution is to add an extra step at the end of the iterative meteor shower extraction. At the end, when all radiants are determined, the shower assignment will be repeated for all meteors. This time, the meteors are not assigned to the strongest radiant, but to the one that fits best. Interference from nearby showers will not show up anymore.

Meteor shower velocities

There have been detailed investigations, why the velocity of fast meteor showers was systematically underestimated in the 2006 analysis. They are described in a dedicated paper (Molau & SonotaCo, 2009). So here only a short summary is given.

The determination of meteor shower velocities is based on a formula taken from Gural (1999) that computes the angular meteor velocity at a certain point in the sky from the velocity v_{inf} of the meteor shower. A basic ingredient for this formula is the begin and end height ($h_b$and h_e) of the meteor, which is unknown in case of single station observations. For this reason, the following estimates have been used in the 2006 analysis:

$$h_b = 100 + v^2_{inf}/200 \qquad h_e = 85 \qquad [2]$$

Experiments showed, that systematic variations of these parameters cause systematic shifts of the determined meteor shower velocities. However, none of these parameters could lift only the velocity of fast showers. Only when the end height was made dependent from the meteor shower velocity v_{inf} in the same way as the begin height, the desired effect could be achieved. The parameter was adjusted such, that the velocity determined for a set of well-known showers matched the expected value best:

$$h_b = 100 + v^2_{inf}/200 \qquad h_e = 75 + v^2_{inf}/200 \qquad [3]$$

To verify the result, double station data from the Japanese SonotaCo network were used. Based on 18,650 meteor trajectories recorded in 2007, the dependency of the begin and end height from the meteor shower velocity was determined. It was confirmed, that both proportional to the meteor shower velocity:

$$h_b = 79 + 0.48*v_{inf} \qquad h_e = 67 + 0.48*v_{inf} \qquad [4]$$

We found a linear dependency and could show that the altitude range h_b-h_e in which meteors show up, is about 12 km independent of the meteor shower velocity. Even though the formulae [3] and [4] look quite different, their output for the average altitude (h_b-h_e/2) differs only slightly for most velocity values.

In further studies we analyzed the impact of other parameters to the average meteor altitude. We found, that:

- the altitude increases by about 1 km per magnitude in the brightness range of m = 0 mag to 3 mag, i.e. brighter meteors are seen at higher altitudes
- the altitude range depends directly from the meteor duration d: h_b-h_e [km] = 38 * d [s]
- the altitude decreases for every 10° of the entry angle ea, which is identical to the radiant altitude, i.e. meteoroids from showers with a low radiant, that enter at a shallow angle, will penetrate deeper into the atmosphere

The resulting formula that account for all effects and that was used in this analysis, is:

$$h_b = 78 + 0.48*v_{inf} + m - ea/10 + 38*d, \qquad h_e = 78 + 0.48*v_{inf} + m - ea/10 - 38*d \qquad [5]$$

Parameter estimation

The following probability distribution used in the 2006 analysis of the video meteor database (Molau, 2006):

$$P(M \mid R) = \exp(-0.5*d^2) * \exp(-1.5*v^2) \qquad [6]$$

Here, d [°] is the radiant miss distance of the backward prolongated meteor, and v [°/s] the deviation between the expected and the observed angular velocity. As the true shape of the probability distribution was unknown, a Gauss distribution was assumed, whereby the standard deviation was set empirically.

In order to improve the analysis, the distribution type and parameters were to be estimated from data. At first, the radiant position of three major showers (PER, ORI, GEM) at their maximum was computed from data. In the second step, the deviation of roughly 33,000 shower meteors that appeared close to the maximum was calculated with respect to position and velocity. It turned out, that the standard deviation was smaller than expected. For 50% or all meteors, the measured angular velocity deviated less than 0.5°/s from the expected velocity, and the radiant miss distances was below 0.75°. Furthermore, the error distribution was not Gaussian, but could be well approximated with a Laplace distribution. The main difference is that for larger values, a Gauss distribution converges much faster to zero than a Laplace distribution.

In a second set of experiments it was tested, in how far the deviations were dependent from the radiant distance and velocity of the meteor. In case of visual observation such dependencies are assumed, which is why in meteor shower assignment larger errors are accepted when the meteor is farther away from the radiant or faster.

It turned out, that the radiant miss distance d is independent of the radiant distance of the meteor (figure 5). The explanation is simple: The farther away, the longer is the meteor, and the longer it is, the smaller are the errors in the determination of the meteor direction. When the begin and end point are nearby, small measurement errors will result in larger errors of the meteor direction, but when they are apart, the meteor direction will be effected less from measurement errors of the begin and end point. That effect compensates for the fact, that small meteor direction errors will result in a large radiant miss distance when the meteor is farther away from the radiant.

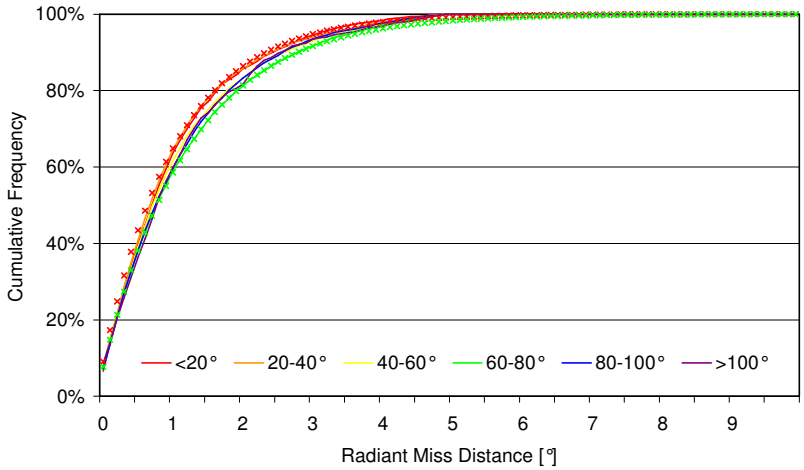

Figure 5: Radiant miss distance distribution depending of the distance of the meteor from the radiant. The error distribution is almost perfectly Laplacian shaped (crosses are individual measurements, lines the corresponding Laplace fits) and there is no dependency from the radiant distance of the meteor.

On the other hand, the distribution of the velocity errors was clearly dependent from the angular meteor velocity (figure 6). The velocity deviation of meteors moving slower than 5°/s was less than half of the deviation of meteors moving faster than 30°/s. The standard deviation of the Laplace distribution was linear dependent from the meteor velocity.

The new probability distribution, which was used for accumulating radiant probabilities in the meteor shower analysis, was as follows:

$$P(M \mid R) = \exp(-0.8*d) * \exp(-v/(0.4+v/50)) \qquad [7]$$

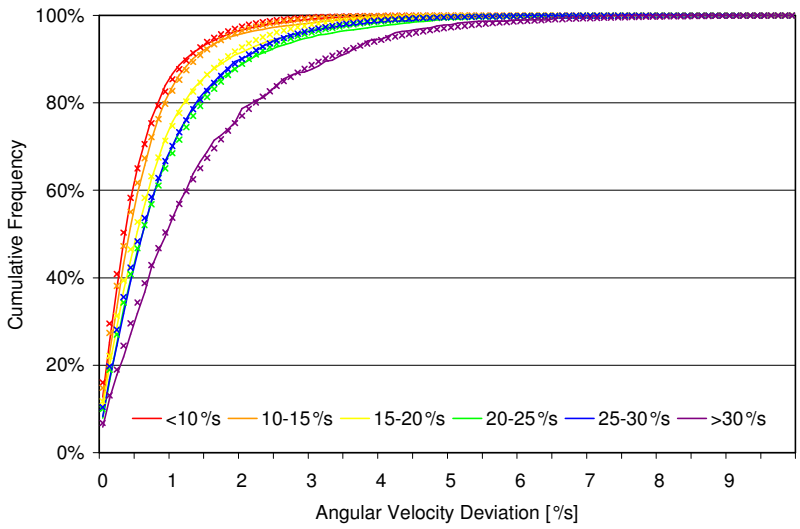

Figure 6: Distribution of the angular velocity deviation depending on the velocity of the meteor. The error distribution is almost perfectly Laplacian shaped (crosses are individual measurements, lines the corresponding Laplace fits) and the deviation between the expected and the observed angular velocity increases,with the meteor velocity.

Data set

The new meteor shower analysis was based on a set of 359,957 meteors recorded between January 1993 and July 2008, i.e. the data set had almost doubled compared to the first analysis in 2006. For each individual solar longitude interval, between 535 meteors (solar longitude 348 / March 7) and 14,641 meteors (solar longitude 236 / November 19) were available (figure 7). Beside the modifications described in the previous chapters, the search routine was not modified.

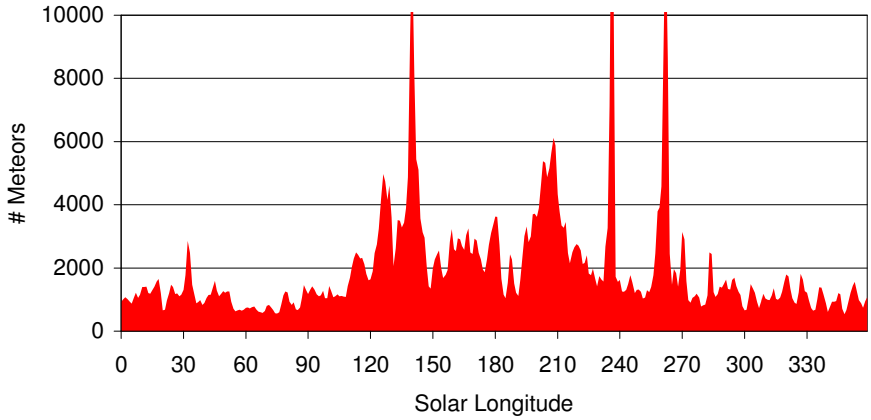

Figure 7: Solar longitude distribution of meteors from the data set used in this analysis.

Results

The activity profiles of all showers from the IMO working list detected in the analysis are plotted in figure 8. On the first look, the relative strengths of some showers seems unlikely: Why should the Orionid maximum be stronger than that of the Perseids? However, it should be noted that the interval length of each data point is two degrees in solar longitude. The Quadrantids, Perseids and Geminids all reach maximum ZHR values beyond 100, but only for a short time. Averaged over two days, their ZHR reduces significantly. The Orionids, on the other hand, experienced strong return in 2006 and 2007, to which most data belong. Their maximum lasts for several days, which is why the Orionid peak is not smeared out. The eta-Aquariids on the other hand, are strongly enhanced due to their low observability probability, which makes their activity value less confident.

Overall it can be stated, that the introduction of the observability function clearly improves the qualitative value of the activity graphs, even if the result is not yet perfect.

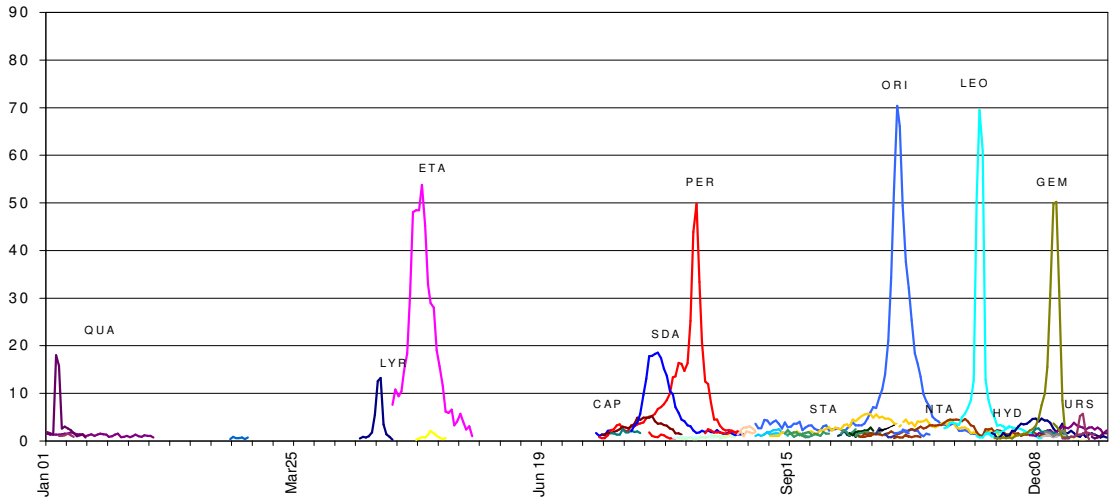

Figure 8: Activity graphs for all detected showers that belong to the IMO working list.

The activity graphs of the southern and northern Taurids are given in figure 9. The interference observed in the 2006 analysis (Molau, 2006) has disappeared thanks to the improved algorithm.

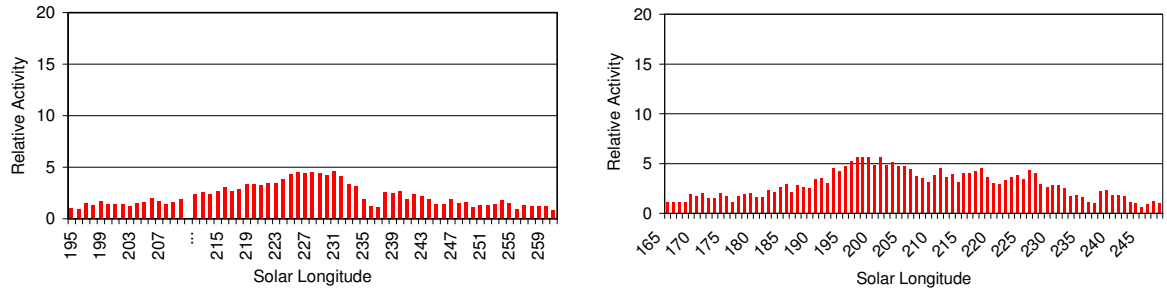

Figure 9: Activity graphs of the northern (left) and southern (right) Taurids.

Also the meteor shower velocities are more reliable with the improved formula for meteor altitudes. Figure 10 compares the measured meteor shower velocities of known showers with the values taken from the IMO working list. The old values from 2006 are marked with green dots, the new values from this analysis with red squares. The aforementioned systematic deviation of fast meteor showers in the old analysis is obvious, but they disappeared in the new analysis.

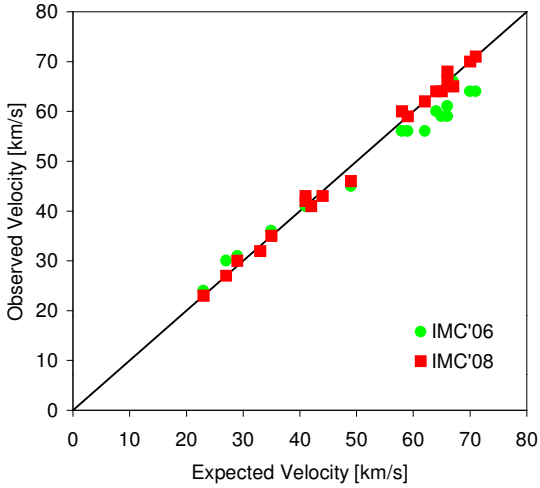

Figure 10: Comparions of the measured meteor shower velocities with the values taken from the IMO working list. The systematic deviation observed in the 2006 analysis has disappeared thanks to the improved algorithm.

The full list of all detected meteor showers is given in Table 1. Note that the table contains the raw output of the detection procedure. There has been no manual verification or correction of the figures.

The columns are as follows:

- ID – arbitrary identifier from the detection algorithm: 08 = ID from this analysis, 06 = ID from the corresponding shower of the 2006 analysis (Molau, 2006)
- Period of Activity – solar longitude interval in which a shower was detected, the corresponding dates, and the overall number of meteors belonging to the shower Maximum Activity - solar longitude and date of maximum activity, maximum activity
- Properties – right ascension, declination, and velocity of the meteor showers at the time of maximum activity
- Drift – average drift in right ascension and declination per day. Beware that the radiant position in solar longitude intervals with low activity is difficult to determine, which is why the drift values may contain large errors
- Remarks - name of the shower or sporadic source, if known

In parenthesis are the reference values from the IMO working list, if available.

Conclusions

In 2006, a first automated meteor shower search in the IMO Video Meteor Database was carried out. Whereas the basic algorithm presented in Molau (2006) has proven to be useful, some weaknesses where detected as well. These issues have been analysed and solved before a new analysis based on a data set almost twice as large has been carried out in 2008. The effectiveness of the proposed solutions could be confirmed.

Acknowledgements

I'm indebted to all members of the IMO Video Meteor Network for their patience and fine work. The resulting database of roughly 350,000 single station video meteors to date is unprecedented and the ultimate basis for all analyses and results presented here. The twenty most active video observers are: Sirko Molau (DE), Jörg Strunk (DE), Javor Kac (SL), Ilkka Yrjölä (FI), Stane Slavec (SL), Orlando Benitez-Sanchez (ES), Jürgen Rendtel (DE), Flavio Castellani (IT), Mihaela Triglav (SL), Stephen Evans (UK), Detlef Koschny (NL), Bernd Brinkmann (DE), Steve Quirk (AU), Enrico Stomeo (IT), Robert Lunsford (US), Wolfgang Hinz (DE), Biondani Roberto (IT), Mirko Nitschke (DE), Stefan Ueberschaer (DE) and Ulrich Sperberg (DE).

References

Arlt R. (1992). „The software Radiant". *WGN*, **20**, 62-69.

Gural P. (1999). „A Rigorous Expression for the Angular Velocity of a Meteor", *WGN*, **27**, 111-114.

Molau S. (2001). „The AKM Video Meteor Network". In: Warmbein B. (ed.), Proc. Meteoroids 2001, 315-318, Kiruna, Sweden.

Molau S. (2006). „How good is the IMO Working List of Meteor Showers? A complete analysis of the IMO Video Meteor Database". In: Bettonvil F., Kac J. (eds.), Proc. Int. Met. Conf. 2006, 38-54, Roden, the Netherlands.

Molau S., SonotaCo (2009). „On the average altitude of (video) meteors". *WGN*, **36**, 124-130.

Table 1: List of meteor showers automatically detected from the IMO Video Meteor Database

ID		Period of Activity			Maximum Activity		Properties				Drift		Name
'08	'06	λ [°]	Date	# Met.	λ [°]	Date	α [°]	δ [°]	Vel. [km/s]	Act.	α °/day	δ °/day	
146	83	274-293 (280-284)	Dec 26-Jan 13 (Jan 01-Jan 05)	1336	283 (282)	Jan 04 (Jan 03)	230.2 (230.0)	49.0 (49.0)	42 (41)	18.0	+0.6 (+0.8)	-0.3 (-0.2)	QUA
147	87	278-283	Dec 30-Jan 04	88	283	Jan 04	172.9	-19.0	67	2.9	-0.4	+0.4	S Apex
148	89	279-291	Dec 31-Jan 11	161	286	Jan 07	128.6	-9.0	40	1.5	+0.6	-0.1	-
149		284-289 (260-303)	Jan 05-Jan 09 (Dec 12-Jan 23)	100	287 (267)	Jan 07 (Dec 19)	187.8 (176.0)	8.0 (24.0)	68 (65)	1.5	+1.6 (+0.8)	+2.1 (-0.3)	COM
150		285-295	Jan 06-Jan 15	253	288	Jan 08	116.4	25.0	25	1.0	+0.2	-0.7	ANT
151	85/90	286-292	Jan 07-Jan 12	136	288	Jan 08	115.7	14.5	27	1.1	+1.1	-1.1	ANT
152		287-293	Jan 07-Jan 13	104	291	Jan 11	215.7	12.0	67	1.6	-3.3	+0.5	N Apex
153		291-298	Jan 11-Jan 18	181	293	Jan 13	130.2	20.5	31	0.9	+0.8	+0.8	ANT
154		300-306	Jan 20-Jan 26	151	301	Jan 21	134.4	21.0	29	1.1	-0.1	-0.6	ANT
155		304-309	Jan 24-Jan 29	100	308	Jan 28	222.7	16.5	68	1.7	-3.1	-0.9	N Apex
156	92	309-314	Jan 29-Feb 03	90	314	Feb 03	157.2	7.0	32	0.7	-0.5	+0.8	Anthel.
157	93	313-318	Feb 02-Feb 07	66	316	Feb 05	163.6	-15.0	46	0.9	+1.2	-0.9	-
158	94	315-322	Feb 04-Feb 11	213	318	Feb 07	153.9	9.0	34	1.2	+1.1	-0.2	ANT
159		318-325	Feb 07-Feb 14	133	324	Feb 13	235.5	0.0	66	1.7	-1.1	-2.1	-
160		322-328	Feb 11-Feb 17	155	325	Feb 14	211.2	6.0	62	1.5	-1.1	-1.4	-
161		322-328	Feb 11-Feb 17	129	324	Feb 13	246.1	23.0	53	1.5	+0.8	-0.7	-
162	95	323-340	Feb 12-Mar 01	373	340	Mar 01	167.3	5.5	27	1.2	-0.1	+0.2	ANT
163		325-331	Feb 14-Feb 20	126	331	Feb 20	175.5	0.0	40	1.0	-1.1	-1.2	ANT
164		330-337	Feb 19-Feb 26	88	335	Feb 24	260.4	41.0	52	0.8	+0.3	+0.7	-
165		335-340	Feb 24-Mar 01	87	335	Feb 24	181.7	2.5	36	0.8	+1.0	-0.1	ANT
166		340-348	Mar 01-Mar 09	80	346	Mar 07	268.3	41.0	42	1.8	+1.1	+1.5	-
167		342-348 (326-349)	Mar 03-Mar 09 (Feb 15-Mar 10)	116	343 (335)	Mar 04 (Feb 24)	163.5 (168.0)	0.5 (16.0)	24 (23)	0.9	+1.4 (+0.9)	+1.2 (-0.3)	DLE
168		349-355	Mar 10-Mar 16	141	352	Mar 13	254.1	48.0	36	1.0	+0.6	-0.9	-
169	(4)	353-359	Mar 14-Mar 20	118	358	Mar 19	200.8	-9.5	36	1.2	+0.2	-2.5	ANT
1	1	357-4	Mar 18-Mar 25	199	0	Mar 21	186.2	2.5	27	1.4	+0.0	+0.0	ANT
2		0-6	Mar 21-Mar 27	120	6	Mar 27	196.7	-15.5	30	1.0	+0.4	-1.2	ANT
3		7-13	Mar 28-Apr 03	144	8	Mar 29	210.8	-13.5	36	1.1	+0.6	-0.2	ANT
4	2	7-24	Mar 28-Apr 14	307	20	Apr 10	302.1	41.0	41	1.3	+0.4	+0.4	-
5		14-23	Apr 04-Apr 13	299	22	Apr 12	204.4	-15.5	25	1.8	+0.2)	-0.1	ANT
6	6	19-27	Apr 09-Apr 17	256	23	Apr 13	214.9	-17.0	29	1.7	-0.2	+0.4	ANT
7		24-29	Apr 14-Apr 19	71	27	Apr 17	292.5	0.0	69	1.2	-0.3	+0.8	N Apex
8	5	26-35	Apr 16-Apr 25	279	29	Apr 19	221.5	-15.0	28	1.3	+0.2	+1.0	ANT
9	7	26-37 (26-35)	Apr 16-Apr 27 (Apr 16-Apr 25)	1516	33 (32)	Apr 23 (Apr 22)	272.5 (271.0)	33.0 (34.0)	46 (49)	13.2	+0.9 (+1.1)	-0.4 (+0.0)	LYR
10		29-49	Apr 19-May 10	401	37	Apr 27	317.2	43.0	44	1.9	+1.5	+0.4	-
11		30-40	Apr 20-May 01	196	37	Apr 27	207.0	-5.5	21	1.4	+0.1	-2.1	-
12		36-43	Apr 26-May 04	91	39	Apr 29	302.5	25.5	57	1.3	+0.0	-0.2	-
13	8	37-47	Apr 27-May 08	218	45	May 06	241.3	-15.5	31	1.4	+1.8	-0.5	ANT
14	9	37-64 (29-67)	Apr 27-May 25 (Apr 19-May 29)	1051	47 (44)	May 08 (May 05)	339.0 (338.0)	-0.5 (-1.0)	68 (66)	53.8	+0.6 (+0.9)	+0.4 (+0.4)	ETA
15		40-45	May 01-May 06	82	41	May 02	307.5	1.0	67	2.1	+1.5	+2.6	N Apex
16	10	45-55 (42-51)	May 06-May 16 (May 03-May 12)	264	50 (48)	May 11 (May 09)	290.6 (287.0)	43.0 (44.0)	43 (44)	2.1	+0.1 (+1.0)	-0.5 (+0.0)	ELY
17		50-57	May 11-May 18	136	56	May 17	245.5	-18.0	30	1.8	-1.2	+0.9	ANT
18		50-55	May 11-May 16	80	53	May 14	310.3	15.5	65	1.4	+0.1	+0.7	N Apex
19		54-60	May 15-May 21	70	59	May 20	240.1	56.5	22	0.5	-4.3	-0.3	-
20		58-63	May 19-May 24	66	61	May 22	223.1	-14.0	17	1.1	+0.0	-1.8	-
21	11	58-68	May 19-May 30	147	67	May 29	254.6	-14.5	30	1.6	-0.2	+0.8	ANT
22	12	70-79	Jun 01-Jun 10	222	77	Jun 08	265.5	-27.5	26	2.4	+1.7	+0.1	ANT
23	14/15	76-90	Jun 07-Jun 22	361	87	Jun 18	275.0	-27.0	25	2.3	+0.4	-0.1	ANT
24	13	78-85	Jun 09-Jun 16	121	85	Jun 16	343.7	25.0	66	1.1	+0.7	+0.6	N Apex
25	16/19	85-120	Jun 16-Jul 23	907	104	Jul 06	312.2	-5.0	43	2.1	+0.7	+0.1	-
26	13	87-127	Jun 18-Jul 30	1658	101	Jul 03	15.3	23.5	70	5.4	+0.8	+0.4	N Apex
27		88-93	Jun 19-Jun 25	94	92	Jun 24	11.1	5.5	71	3.6	+0.3	+0.8	-
28	18	96-115	Jun 28-Jul 18	552	110	Jul 13	32.0	49.0	59	2.3	+1.1	+0.4	-
29	(17)	97-108	Jun 29-Jul 10	246	107	Jul 09	288.1	-21.0	26	2.4	-0.1	+0.2	ANT
30		99-106	Jul 01-Jul 08	95	103	Jul 05	269.4	13.5	21	0.7	+0.7	-1.7	-

31		104-128	Jul 06-Jul 31	591	108	Jul 10	347.9	11.0	67	1.6	+0.9	+0.3	-
32		106-111 (110-146)	Jul 08-Jul 14 (Jul 13-Aug 19)	78	111 (125)	Jul 14 (Jul 28)	329.2 (339.0)	-29.5 (-16.0)	39 (41)	2.2	+1.1 (+1.0)	+0.0 (+0.3)	SDA
33		107-154 (114-151)	Jul 09-Aug 27 (Jul 17-Aug 24)	17872	140 (139)	Aug 13 (Aug 12)	47.5 (46.0)	57.5 (58.0)	59 (59)	49.8	+1.5 (+1.3)	+0.2 (+0.2)	PER
34	20	108-135 (101-142)	Jul 10-Aug 08 (Jul 03-Aug 15)	1979	125 (127)	Jul 28 (Jul 30)	305.1 (308.0)	-10.0 (-10.0)	24 (23)	5.2	+0.5 (+1.0)	+0.2 (+0.3)	CAP
35	22/26	111-121 (114-151)	Jul 14-Jul 24 (Jul 17-Aug 24)	438	115 (139)	Jul 18 (Aug 12)	21.2 (46.0)	45.0 (58.0)	66 (59)	2.4	+0.4 (+1.3)	-0.1 (+0.2)	PER
36		113-118	Jul 16-Jul 21	129	117	Jul 20	272.8	39.0	21	0.6	+0.0	-0.5	-
37		116-121	Jul 19-Jul 24	128	121	Jul 24	0.0	41.0	52	0.7	-1.0	-1.3	-
38	25	118-156 (110-146)	Jul 21-Aug 30 (Jul 13-Aug 19)	4101	127 (125)	Jul 30 (Jul 28)	340.5 (339.0)	-16.5 (-16.0)	43 (41)	18.5	+0.9 (+1.0)	+0.3 (+0.3)	SDA
39		119-124	Jul 22-Jul 27	192	120	Jul 23	30.3	29.0	71	3.6	-0.1	-2.2	-
40		119-128	Jul 22-Jul 31	383	125	Jul 28	281.4	50.5	28	1.6	-0.2	+0.3	-
41	27	120-145	Jul 23-Aug 18	1524	123	Jul 26	31.8	39.5	66	3.6	+0.8	+0.0	N Apex
42		122-127	Jul 25-Jul 30	148	122	Jul 25	249.5	66.0	23	0.6	+5.6	+0.8	-
43	28	122-130	Jul 25-Aug 02	261	122	Jul 25	320.8	-17.5	35	1.4	-1.0	+0.7	ANT
44		124-133 (114-151)	Jul 27-Aug 06 (Jul 17-Aug 24)	405	124 (139)	Jul 27 (Aug 12)	27.6 (46.0)	59.5 (58.0)	57 (59)	1.8	-2.1 (+1.3)	+0.9 (+0.2)	PER
45		125-143	Jul 28-Aug 16	495	128	Jul 31	35.2	-15.0	66	5.3	+0.7	+0.5	S Apex
46		129-138	Aug 01-Aug 11	234	131	Aug 04	6.3	17.0	67	1.0	+0.8	+0.5	-
47	(30)	129-134	Aug 01-Aug 07	196	132	Aug 05	327.5	-9.5	32	1.7	+0.9	-0.3	ANT
48		132-149 (131-152)	Aug 05-Aug 22 (Aug 04-Aug 25)	749	144 (144)	Aug 17 (Aug 17)	288.3 (190.0)	52.5 (-5.2)	23 (25)	1.1	+0.9 (+0.0)	+0.2 (+0.0)	KCG
49		134-144 (131-152)	Aug 07-Aug 17 (Aug 04-Aug 25)	393	144 (144)	Aug 17 (Aug 17)	266.4 (286.0)	62.5 (59.0)	21 (25)	0.9	-1.0 (+0.0)	+0.8 (+0.0)	KCG
50		134-141	Aug 07-Aug 14	382	137	Aug 10	32.8	33.0	65	1.6	+0.1	-0.3	N Apex
51	33	135-164	Aug 08-Sep 07	1346	148	Aug 21	353.3	5.0	40	2.2	+0.5	+0.1	Anthel.
52	(36)	141-151	Aug 14-Aug 24	276	149	Aug 22	330.3	-12.5	21	1.5	+0.5	+0.7	ANT
53		142-147	Aug 15-Aug 20	242	147	Aug 20	344.8	-10.5	30	2.4	+1.0	-1.5	ANT
54		143-155 (114-151)	Aug 16-Aug 28 (Jul 17-Aug 24)	542	144 (139)	Aug 17 (Aug 12)	53.7 (46.0)	33.0 (58.0)	66 (59)	2.5	+1.0 (+1.3)	+0.4 (+0.2)	PER
55	32/37	145-152 (131-152)	Aug 18-Aug 25 (Aug 04-Aug 25)	308	145 (144)	Aug 18 (Aug 17)	277.4 (286.0)	58.0 (59.0)	23 (25)	1.2	-1.8 (+0.0)	+0.5 (+0.0)	KCG
56		148-153 (131-152)	Aug 21-Aug 26 (Aug 04-Aug 25)	175	151 (144)	Aug 24 (Aug 17)	290.0 (286.0)	58.5 (59.0)	24 (25)	1.0	+0.7 (+0.0)	+0.0 (+0.0)	KCG
57		150-161	Aug 23-Sep 04	395	161	Sep 04	42.0	42.5	71	1.2	+1.0	-0.4	N Apex
58		150-157	Aug 23-Aug 31	166	157	Aug 31	336.7	-6.5	25	1.3	+0.1	-0.5)	ANT
59		150-156	Aug 23-Aug 30	187	155	Aug 28	49.7	19.0	65	1.9	+0.8	-1.5	N Apex
60	(43)	151-157	Aug 24-Aug 31	150	153	Aug 26	55.1	-3.5	67	3.0	-1.0	+2.9	S Apex
61	38	151-160	Aug 24-Sep 03	379	156	Aug 30	68.9	41.0	63	2.0	-1.2	-0.8	N Apex
62		154-160 (152-165)	Aug 27-Sep 03 (Aug 25-Sep 08)	144	155 (158)	Aug 28 (Sep 01)	97.7 (91.0)	45.5 (39.0)	59 (67)	2.0	+3.7 (+0.0)	-1.2 (+0.0)	AUR
63	42	154-161	Aug 27-Sep 04	220	157	Aug 31	347.8	2.5	30	1.5	-0.7	+0.0	ANT
64		155-160 (152-165)	Aug 28-Sep 03 (Aug 25-Sep 08)	240	158 (158)	Sep 01 (Sep 01)	91.4 (91.0)	38.5 (39.0)	65 (67)	3.1	+1.3 (+0.0)	+0.0 (+0.0)	AUR
65		157-162	Aug 31-Sep 05	190	160	Sep 03	280.1	57.5	22	0.8	-2.4	-0.6	-
66	46	157-163	Aug 31-Sep 06	192	163	Sep 06	10.5	-4.0	37	1.3	+0.2	-0.9	-
67	57	160-239 (189-224)	Sep 03-Nov 21 (Oct 02-Nov 07)	14012	208 (207)	Oct 22 (Oct 21)	95.5 (95.0)	15.5 (16.0)	68 (66)	70.4	+0.7 (+0.7)	+0.2 (+0.1)	ORI
68	47	160-171 (162-174)	Sep 03-Sep 14 (Sep 05-Sep 17)	760	168 (166)	Sep 11 (Sep 09)	48.0 (59.0)	39.5 (47.0)	65 (64)	2.5	+0.3 (+1.1)	+1.1 (+0.1)	SPE
69		163-168 (162-174)	Sep 06-Sep 11 (Sep 05-Sep 17)	315	164 (166)	Sep 07 (Sep 09)	79.9 (59.0)	46.5 (47.0)	65 (64)	1.8	+1.2 (+1.1)	-0.1 (+0.1)	SPE
70	53	165-248 (182-210)	Sep 08-Nov 30 (Sep 25-Oct 24)	6823	198 (197)	Oct 11 (Oct 10)	34.4 (32.0)	9.0 (9.0)	29 (27)	5.7	+0.8 (+0.7)	+0.2 (+0.3)	STA
71		166-174	Sep 09-Sep 17	349	166	Sep 09	1.0	4.0	30	1.7	-1.1	-1.2	ANT
72	49	166-172	Sep 09-Sep 15	265	170	Sep 13	112.7	56.0	58	1.6	+2.4	+0.8	-
73		166-176	Sep 09-Sep 19	241	169	Sep 12	284.0	61.5	23	0.7	-1.6	+0.5	-
74		168-173	Sep 11-Sep 16	183	172	Sep 15	286.5	89.0	41	0.8	-8.9	+0.9	N Toro
75	51	169-174	Sep 12-Sep 17	190	173	Sep 16	17.2	8.5	39	1.3	+0.4	+1.8	ANT
76		170-182	Sep 13-Sep 25	372	175	Sep 18	290.8	80.0	34	0.8	-2.8	+0.7	-
77		170-179 (175-197)	Sep 13-Sep 22 (Sep 18-Oct 10)	484	171 (191)	Sep 14 (Oct 04)	75.4 (88.0)	38.5 (49.0)	70 (64)	2.3	-0.7 (+1.0)	-0.1 (+0.0)	DAU
78		171-178	Sep 14-Sep 21	310	172	Sep 15	54.6	38.0	65	1.5	-0.7	-0.9	DAU

		(175-197)	(Sep 18-Oct 10)		(191)	(Oct 04)	(88.0)	(49.0)	(64)		(+1.0)	(+0.0)	
79		176-181 (175-197)	Sep 19-Sep 24 (Sep 18-Oct 10)	345	181 (191)	Sep 24 (Oct 04)	72.6 (88.0)	47.0 (49.0)	69 (64)	1.4	+2.7 (+1.0)	+1.8 (+0.0)	DAU
80		178-183	Sep 21-Sep 26	152	182	Sep 25	128.9	77.0	47	0.6	-6.7	+0.5	-
81		180-185 (175-197)	Sep 23-Sep 28 (Sep 18-Oct 10)	260	183 (191)	Sep 26 (Oct 04)	96.9 (88.0)	45.0 (49.0)	66 (64)	1.9	+0.3 (+1.0)	-0.4 (+0.0)	DAU
82		182-191	Sep 25-Oct 04	275	191	Oct 04	97.7	34.0	55	2.0	+0.5	+0.3	N Apex
83		185-195	Sep 28-Oct 08	214	194	Oct 07	14.8	11.5	27	1.2	+3.0	+1.4	-
84		186-191	Sep 29-Oct 04	59	186	Sep 29	312.1	36.0	16	0.5	+2.1	-0.2	-
85		187-194	Sep 30-Oct 07	195	192	Oct 05	96.2	4.0	71	2.7	+0.6	+0.2	S Apex
86	56	188-195 (182-210)	Oct 01-Oct 08 (Sep 25-Oct 24)	326	190 (197)	Oct 03 (Oct 10)	18.8 (30.0)	17.0 (15.0)	31 (29)	2.2	+0.8 (+0.8)	-0.6 (+0.3)	NTA
87		189-194 (189-224)	Oct 02-Oct 07 (Oct 02-Nov 07)	166	194 (207)	Oct 07 (Oct 21)	99.9 (95.0)	17.0 (16.0)	71 (66)	2.5	+1.6 (+0.7)	-0.4 (+0.1)	ORI
88	58	192-200 (199-213)	Oct 05-Oct 14 (Oct 12-Oct 27)	491	199 (204)	Oct 12 (Oct 18)	95.8 (102.0)	27.5 (27.0)	70 (70)	2.8	+0.1 (+1.0)	-1.8 (+0.0)	EGE
89		193-198	Oct 06-Oct 11	157	195	Oct 08	109.7	3.0	71	2.7	-0.3	+1.0	-
90	60	194-204 (175-197)	Oct 07-Oct 18 (Sep 18-Oct 10)	597	198 (191)	Oct 11 (Oct 04)	108.7 (88.0)	44.5 (49.0)	69 (64)	1.9	+0.0 (+1.0)	-0.6 (+0.0)	DAU
91	(59)	194-206	Oct 07-Oct 20	455	195	Oct 08	172.1	85.5	41	0.9	-0.7	-1.0	-
92		195-200 (182-210)	Oct 08-Oct 14 (Sep 25-Oct 24)	289	200 (197)	Oct 14 (Oct 10)	32.6 (30.0)	20.5 (15.0)	38 (29)	1.5	-1.1 (+0.8)	+0.6 (+0.3)	NTA
93		195-210 (182-210)	Oct 08-Oct 24 (Sep 25-Oct 24)	973	206 (197)	Oct 20 (Oct 10)	38.5 (30.0)	18.5 (15.0)	30 (29)	2.0	+1.6 (+0.8)	+0.5 (+0.3)	NTA
94		195-200	Oct 08-Oct 14	209	195	Oct 08	98.7	-4.0	64	3.3	-1.2	-0.6	S Apex
95		197-221	Oct 10-Nov 04	1001	200	Oct 14	130.9	29.0	67	3.7	+0.7	+0.0	-
96		201-208 (199-204)	Oct 15-Oct 22 (Oct 12-Oct 18)	468	202 (202)	Oct 16 (Oct 16)	144.0 (144.0)	64.5 (64.0)	54 (51)	2.7	+1.6 (+1.5)	-1.1 (-0.5)	TUM
97		201-209	Oct 15-Oct 23	390	207	Oct 21	134.1	45.5	70	1.6	+0.9	+0.8	N Apex
98		202-207 (199-213)	Oct 16-Oct 21 (Oct 12-Oct 27)	551	207 (204)	Oct 21 (Oct 18)	102.0 (102.0)	27.5 (27.0)	71 (70)	3.2	+0.3 (+1.0)	-0.3 (+0.0)	EGE
99		203-208	Oct 17-Oct 22	132	203	Oct 17	346.6	52.5	25	0.5	-4.6	+1.4	-
100	63	203-213 (205-213)	Oct 17-Oct 27 (Oct 19-Oct 27)	421	209 (210)	Oct 23 (Oct 24)	159.9 (162.0)	36.5 (37.0)	61 (62)	3.8	+1.1 (+1.0)	-0.2 (-0.4)	LMI
101		207-212 (211-243)	Oct 21-Oct 26 (Oct 25-Nov 25)	191	211 (227)	Oct 25 (Nov 10)	52.0 (56.0)	22.5 (22.0)	35 (29)	1.3	+0.7 (+0.9)	+0.3 (+0.2)	NTA
102		207-212 (189-224)	Oct 21-Oct 26 (Oct 02-Nov 07)	273	210 (207)	Oct 24 (Oct 21)	88.3 (96.0)	13.0 (16.0)	64 (66)	2.1	+1.2 (+0.7)	-1.4 (+0.1)	ORI
103		210-219 (189-224)	Oct 24-Nov 02 (Oct 02-Nov 07)	428	213 (207)	Oct 27 (Oct 21)	107.7 (95.0)	27.5 (16.0)	71 (66)	2.5	+0.4 (+0.7)	+1.3 (+0.1)	ORI
104		210-216	Oct 24-Oct 30	191	210	Oct 24	117.7	45.5	65	2.3	-1.4	+1.1	N Apex
105		211-216 (211-243)	Oct 25-Oct 30 (Oct 25-Nov 25)	185	211 (227)	Oct 25 (Nov 10)	32.0 (56.0)	29.0 (22.0)	27 (29)	1.1	-0.9 (+0.9)	-3.0 (+0.2)	NTA
106	62	212-261 (211-243)	Oct 26-Dec 13 (Oct 25-Nov 25)	3417	231 (227)	Nov 14 (Nov 10)	59.2 (56.0)	23.0 (22.0)	29 (29)	4.6	+0.9 (+0.9)	+0.1 (+0.2)	NTA
107		213-220	Oct 27-Nov 03	175	214	Oct 28	110.5	-5.5	62	2.8	+1.6	+0.2	S Apex
108		213-218	Oct 27-Nov 01	109	216	Oct 30	145.5	78.5	43	0.8	+1.7	-0.3	-
109	(65)	217-223	Oct 31-Nov 06	194	222	Nov 05	151.3	37.5	64	2.2	-0.3	-1.1	N Apex
110	69	218-236	Nov 01-Nov 19	429	222	Nov 05	23.1	30.0	19	0.9	+0.1	+0.8	-
111		220-225	Nov 03-Nov 08	147	221	Nov 04	161.5	68.0	48	1.0	+0.2	-1.0	-
112		221-226	Nov 04-Nov 09	191	226	Nov 09	111.5	33.5	69	1.5	-2.4	+0.0	N Apex
113	68	223-228	Nov 06-Nov 11	229	225	Nov 08	146.4	45.0	62	2.7	+0.9	-0.7	N Apex
114		223-234	Nov 06-Nov 17	303	229	Nov 12	47.1	19.0	24	1.2	+0.7	+0.2	-
115	70	224-246 (227-241)	Nov 07-Nov 28 (Nov 10-Nov 23)	8788	236 (234)	Nov 19 (Nov 17)	154.2 (151.0)	21.5 (22.0)	71 (71)	69.5	+0.6 (+0.7)	-0.4 (-0.4)	LEO
116		231-238	Nov 14-Nov 21	193	232	Nov 15	58.1	-3.5	26	1.0	+0.0	-0.4	-
117		231-237	Nov 14-Nov 20	142	233	Nov 16	133.5	-26.0	57	3.2	+1.7	-0.5	-
118	72	235-257 (245-265)	Nov 18-Dec 09 (Nov 27-Dec 17)	855	246 (257)	Nov 28 (Dec 09)	90.8 (103.0)	15.5 (8.0)	45 (42)	3.1	+0.9 (+0.9)	+0.1 (+0.0)	MON
119		236-242	Nov 19-Nov 24	238	241	Nov 23	130.1	31.0	67	1.6	+0.9	+0.2	-
120		238-243 (227-241)	Nov 21-Nov 25 (Nov 10-Nov 23)	96	239 (234)	Nov 21 (Nov 17)	144.8 (151.0)	27.0 (22.0)	57 (71)	1.5	-1.6 (+0.7)	-2.1 (-0.4)	LEO
121	74	240-279 (251-263)	Nov 22-Dec 31 (Dec 03-Dec 15)	1382	257 (260)	Dec 09 (Dec 12)	126.2 (128.0)	3.0 (2.0)	60 (58)	4.7	+0.8 (+0.8)	-0.2 (-0.2)	HYD
122	73/78	241-265	Nov 23-Dec 17	681	253	Dec 05	203.1	60.5	43	1.9	+0.7	-0.5	-
123	75	241-269	Nov 23-Dec 21	12103	262	Dec 14	113.8	32.0	35	50.2	+1.1	-0.1	GEM

		(255-265)	(Dec 07-Dec 17)		(262)	(Dec 14)	(112.0)	(33.0)	(35)		(+1.0)	(-0.1)	
124		244-249	Nov 26-Dec 01	126	248	Nov 30	142.2	-3.0	67	2.8	-1.2	+0.0	S Apex
125		249-256	Dec 01-Dec 08	186	254	Dec 06	169.6	43.5	62	2.2	+1.3	-0.3	N Apex
126		250-259	Dec 02-Dec 11	171	251	Dec 03	182.8	12.5	70	2.6	-1.7	-0.2	N Apex
127		250-255	Dec 02-Dec 07	94	254	Dec 06	165.1	30.0	71	1.8	-1.1	-0.5	-
128		251-258	Dec 03-Dec 10	115	256	Dec 08	158.8	-3.5	70	2.1	+0.4	-0.9	-
129	79	252-257	Dec 04-Dec 09	143	257	Dec 09	89.4	18.0	27	1.4	+0.9	+0.5	ANT
130	76	253-316	Dec 05-Feb 05	2328	268	Dec 20	161.9	30.5	64	3.8	+0.9	-0.4	COM
		(260-303)	(Dec 12-Jan 23)		(267)	(Dec 19)	(176.0)	(24.0)	(65)		(+0.8)	(-0.3)	
131	77	254-268	Dec 06-Dec 20	630	255	Dec 07	98.2	9.0	41	2.6	+0.7	-0.2	MON
		(245-265)	(Nov 27-Dec 17)		(257)	(Dec 09)	(103.0)	(8.0)	(42)		(+0.9)	(+0.0)	
132	(80)	257-265	Dec 09-Dec 17	298	259	Dec 11	176.3	39.0	58	1.2	-0.3	-0.6	COM
		(260-303)	(Dec 12-Jan 23)		(267)	(Dec 19)	(176.0)	(24.0)	(65)		(+0.8)	(-0.3)	
133	(81)	258-265	Dec 10-Dec 17	331	264	Dec 16	177.2	20.0	69	2.3	+1.5	-1.0	COM
		(260-303)	(Dec 12-Jan 23)		(267)	(Dec 19)	(176.0)	(24.0)	(65)		(+0.8)	(-0.3)	
134		258-263	Dec 10-Dec 15	118	259	Dec 11	20.9	66.0	20	0.5	+2.0	-1.4	-
135		259-271	Dec 11-Dec 23	235	260	Dec 12	189.1	-9.5	69	3.5	+0.7	-0.3	-
136		261-266	Dec 13-Dec 18	738	261	Dec 13	108.3	27.0	35	3.7	-0.3	+1.0	GEM
		(255-265)	(Dec 07-Dec 17)		(262)	(Dec 14)	(112.0)	(33.0)	(35)		(+1.0)	(-0.1)	
137		262-267	Dec 14-Dec 19	146	263	Dec 15	86.3	38.0	23	0.5	-0.1	+0.6	-
138	82	263-268	Dec 15-Dec 20	117	264	Dec 16	201.5	8.0	71	2.6	-0.3	+1.0	-
139	82a	264-273	Dec 16-Dec 25	753	271	Dec 23	218.3	75.0	32	5.7	+1.6	-0.2	URS
		(265-274)	(Dec 17-Dec 26)		(270)	(Dec 22)	(217.0)	(75.0)	(33)		(+0.0)	(-0.4)	
140		265-274	Dec 17-Dec 26	235	269	Dec 21	100.0	20.0	27	1.2	-1.2	+1.3	ANT
141		267-272	Dec 19-Dec 24	109	268	Dec 20	234.1	83.5	27	0.5	7.6	-1.2	URS
		(265-274)	(Dec 17-Dec 26)		(270)	(Dec 22)	(217.0)	(75.0)	(33)		(+0.0)	(-0.4)	
142		267-275	Dec 19-Dec 27	227	272	Dec 24	170.2	13.5	69	1.9	+1.6	+0.3	COM
		(260-303)	(Dec 12-Jan 23)		(267)	(Dec 19)	(176.0)	(24)	(65)		(+0.8)	(-0.3)	
143		272-277	Dec 24-Dec 29	114	274	Dec 26	103.0	25.5	31	0.9	-1.1	+0.3	ANT
144		272-277	Dec 24-Dec 29	69	273	Dec 25	173.6	-24.5	65	4.3	-0.7	-0.4	S Apex
145		273-281	Dec 25-Jan 02	99	277	Dec 29	213.5	-0.5	69	3.5	+0.7	+0.1	-